No. 1A-2 $KNbO_3$, Potassium niobate
(M = 180.00)

1a Ferroelectricity in $KNbO_3$ was first discovered by Matthias in 1949. 49Mat

b

phase	IV	III	II	I	
state	F	F	F	P	[a] 63Kat
crystal system	rhombohedral	orthorhombic	tetragonal	cubic	[b] 73Hew
space group	R3m – C_{3v}^{5} [b]	Bmm2 – C_{2v}^{14} [a]	Pamm – C_{4v}^{1} [b]	Pm3m – O_h^{1} [c]	[c] 51Woo
Θ [d] [°C]		–10	225	418(5)	[d] 54Shi1

P_s || [001] in phase II (along [001] of phase I), 49Mat
P_s || [001] in phase III (along [110] of phase I),
P_s || [111] in phase IV (along [111] of phase I).

T_{melt} = 1050 °C. 55Rei, 58Mil

$\rho = 4.62 \cdot 10^3$ kg m^{-3}. 72Pha
Transparent. Light yellow. 67Kat

2a Crystal growth:
Flux method (flux: K_2CO_3). 51Woo
Pulling method from the K_2CO_3–Nb_2O_5 mixture. 58Mil, 72Fuk, 74Fuk1

Top-seeded solution technique. 71Hur, 86WuE

Sol-gel method. 90Naz
Thin film: see 95Gop, 94Der

Phase diagram of the K_2CO_3–Nb_2O_5 system: see 55Rei

b Crystal form: square plate. 58Mil
See also Fig. 1A-2-047 in 15a.

3a Unit cell parameters:
phase II: a = 3.997 Å , c = 4.063 Å at 270 °C. 73Hew

phase III: a = 3.973 Å , b = 5.695 Å ≈ $\sqrt{2}\,a$, c = 5.721 Å ≈ $\sqrt{2}\,a$ at 22 °C.

phase IV: $a = b = c$ = 4.016 Å , $\alpha = \beta = \gamma$ = 89.817(9)° at –43 °C.

b Z = 1 in phases I, II, IV; Z = 2 in phase III. 67Kat, 73Hew

Crystal structure: Table 1A-2-001, Table 1A-2-002, Table 1A-2-003.

4 Temperature dependence of lattice parameters: Table 1A-2-004.

5a Dielectric constant: Figs. 1A-2-001, 1A-2-002, 1A-2-003, 1A-2-004, 1A-2-005, 1A-2-006.
Dielectric constant obtained from hyper-Raman spectra: Fig. 1A-2-007.
See also Table 1A-2-005, Table 1A-2-006.
$\kappa = C / (T - \Theta_p)$, $T > \Theta_{II–I}$, where $C = 2.42 \cdot 10^5$ K, Θ_p = 360(5) °C. 56Tri

$d\Theta_{II–I}/dp = -79$ K G Pa^{-1}. 87Sam

b	Nonlinear dielectric properties: $\xi = -1.7 \cdot 10^9$ VC^{-3}m^5, $\zeta = 2.1 \cdot 10^{10}$ VC^{-5}m^9.	91Cro
c	Spontaneous polarization and coercive field: Fig. 1A-2-008.	
	Measurement using Camlibel pulse method [a]) shows $P_s = 0.41(2)$ Cm^{-2} at RT, which is much larger than the value 0.31 Cm^{-2} obtained by dielectric hysteresis loop.[b])	[a]) 77Gun [b]) 56Tri
	Thin film (320 nm thick): $P_r = 4.5 \cdot 10^{-2}$ Cm^{-2}, $P_s = 4.5 \cdot 10^{-2}$ Cm^{-2},	
	$E_c = 5.5 \cdot 10^6$ Vm^{-1} at 25 °C at 1 kHz.	90Tut
d	Pyroelectric effect: Fig. 1A-2-009; see also	81Pro
6a	Transition heat, transition entropy: Table 1A-2-007.	
7a	Piezoelectricity: Table 1A-2-005, Table 1A-2-006; Fig. 1A-2-010.	
8a	Elastic stiffness: Table 1A-2-005, Table 1A-2-006, Table 1A-2-008; Fig. 1A-2-011.	
	See also	72Pha
9a	Refractive indices: Fig. 1A-2-012, Fig. 1A-2-013; Table 1A-2-009.	
	See also	93Zgo
	Refractive index dispersion on thin film: see	95Gop
	Refractive index of He^+ ion-implanted $KNbO_3$: see	93Flu, 90Zha
	Birefringence: Fig. 1A-2-014, Fig. 1A-2-015.	
	Reflectivity: Fig. 1A-2-016.	
	Dielectric constant in UV region: Fig. 1A-2-017.	
	Infrared reflectivity: Fig. 1A-2-018.	
	Optical absorption: Fig. 1A-2-019; see also	90Mat
b	Electrooptic effect: Table 1A-2-010, Table 1A-2-011; Fig. 1A-2-020, Fig. 1A-2-021, Fig. 1A-2-022.	
	Longitudinal half-wave voltage V_π vs. λ in the obliquely cut crystal; minimal V_π at RT: 195(8) V for $\lambda = 633$ nm, 118(7) V for $\lambda = 458$ nm.	89Ing
e	Nonlinear optical susceptibility : Fig. 1A-2-023.	
	$d_{31} / \lvert d_{11}^{\text{quartz}} \rvert = 35$, $d_{32} / \lvert d_{11}^{\text{quartz}} \rvert = -40$, $d_{33} / \lvert d_{11}^{\text{quartz}} \rvert = -61$ at RT for $\lambda = 1.06$ μm.	74Uem
	Nonlinear optical properties : Fig. 1A-2-024, Fig. 1A-2-025.	
10a	Raman scattering: Fig. 1A-2-026, Fig. 1A-2-027, Fig. 1A-2-028, Fig. 1A-2-029.	
	Optical mode frequencies: Fig. 1A-2-030, Fig. 1A-2-031.	
	Dielectric loss obtained from hyper-Raman scattering: see Fig. 1A-2-07 in 5a.	
	Raman scattering under hydrostatic pressure: Fig. 1A-2-032, Fig. 1A-2-033.	
b	Brillouin scattering (elastic constant): see Table 1A-2-008 in 8a.	
11	Electrical conductivity: Fig. 1A-2-034.	
	Thermoelectric force coefficient vs. T: see	78Han
	Photoelectric character: see	77Rae
	Photorefractive properties:	78Gun, 83Gun, 91Ree, 91Law
	X-ray photoelectron spectra: Fig. 1A-2-035, Fig. 1A-2-036; Table 1A-2-012; see also	92Neu, 94Dou

	Band gap: $E_g \approx 3.3$ eV; information on the electronic band structure: see	76Mic, 78Per, 90XuY, 93Res, 94Kin, 96Sin
13a	NQR: Table 1A-2-013; Figs. 1A-2-037, 1A-2-038, 1A-2-039, 1A-2-040, 1A-2-041.	
b	ESR: Table 1A-2-014. See also	 89Pos
14b	Diffuse X-ray scattering related to elastic stiffness: see Diffuse X-ray scattering in reciprocal space: see	72Pha 68Com1, 68Com2, 70Com, 71Com
	Neutron inelastic scattering: Figs. 1A-2-042, 1A-2-043, 1A-2-044, 1A-2-045, 1A-2-046.	
15a	Domain structure: Fig. 1A-2-047, Fig. 1A-2-048. Domain structure observed by interferometric method: see Domain walls by high resolution electron microscopy: see	 71Des 83Bur
16	Surface charge layers and electroluminescence: see Photorefractive effect: Fig. 1A-2-049; Fig. 1A-2-050; see also Photorefractive properties of undoped, Ta, Na, Rb, Fe doped $KNbO_3$: see Photorefractive electric field in Ta doped $KNbO_3$: see	72Kat 83Gun 91Ree 91Law

Table 1A-2-001. $KNbO_3$. Fractional coordinates and temperature parameters of atoms in the unit cell of phase II [73Hew]. β_{ij} is defined by Eq. (c) in Introduction. Single crystal neutron refinement at 270 °C. For powder neutron profile refinement see [73Hew].

Atom	*x*	*y*	*z*	Δ_z	β_{11} [Å^2]	β_{22} [Å^2]	β_{33} [Å^2]
K	0	0	Δ(K)	0.023(10)	1.66(39)	1.66	1.18(47)
Nb	½	½	½+Δ(Nb)	0	0.79(16)	0.79	0.24(16)
O_I	½	½	$\Delta(O_I)$	0.040(3)	0.95(24)	0.95	1.26(47)
O_{II}	½	0	½+$\Delta(O_{II})$	0.042(3)	0.87(24)	0.79(8)	1.26(45)
O_{III}	0	½	½+$\Delta(O_{II})$	$\Delta(O_{III}) \equiv \Delta(O_{II})$	0.79	0.87	1.26

Table 1A-2-002. $KNbO_3$. Fractional coordinates and temperature parameters of atoms in the unit cell of phase III [73Hew]. β_{ij} is defined by Eq. (c) in Introduction. Powder neutron profile refinement at 22 °C. For single crystal X-ray refinement see [67Kat].

Atom	x	y	z	x	y	z	Δ_z, Δ_y		β_{11} [Å^2]	β_{22} [Å^2]	β_{33} [Å^2]
K	0	0	Δ_z(K)	0	½	½+Δ_z(K)	Δ_z	0.0138(71)	0.52(11)	0.63(24)	0.71(36)
Nb	½	0	½+Δ_z(Nb)	½	½	Δ_z(Nb)	Δ_z	0	0.38(5)	0.33(11)	0.15(28)
O_I	0	0	½+ Δ_z(O_I)	0	½	Δ_z(O_I)	Δ_z	0.0364(10)	0.12(7)	0.63(20)	0.80(35)
O_{II}	½	¼+Δ_y(O_{II})	¼+Δ_z(O_{II})	½	¾+Δ_y(O_{II})	¾+Δ_z(O_{II})	Δ_z	0.0342(9)	0.69(5)	0.47(12)	0.30(21)
							Δ_y	−0.0024(9)	0.69	0.47	0.30
O_{III}	½	¾−Δ_y(O_{II})	¼+Δ_z(O_{II})	½	¾−Δ_y(O_{II})	¾+Δ_z(O_{II})					0.14(12) *)

*) $\beta_{23}(O_{II}) = -\beta_{23}(O_{III})$.

Table 1A-2-003. $KNbO_3$. Fractional coordinates and temperature parameters of atoms in the unit cell of phase IV [73Hew]. β_{ij} is defined by Eq. (c) in Introduction. Powder neutron profile refinement at −37 °C.

Atom	*x*	*y*	*z*		Isotropic	Anisotropic	Isotropic	Anisotropic
				Δ_z, Δ_x			$B(\kappa)$ [Å^2]	β_{ij} [Å^2]
K	Δ_z(K)	Δ_z(K)	Δ_z(K)	Δ_z	0.0112(25)	0.0130(81)	0.49(5)	0.51
							–	0.16 *)
Nb	½+Δ_z(Nb)	½+Δ_z(Nb)	½+Δ_z(Nb)	Δ_z	0	0	0.15(5)	0.15
							–	0.10 *)
O_I	½+Δ_x(O_I)	½+Δ_x(O_I)	Δ_z(O_I)	Δ_x	0.0295(5)	0.0301(9)	0.34(3)	0.46
				Δ_z	0.0308(7)	0.0333(15)	–	0.15(19) *)
O_{II}	½+Δ_x(O_I)	Δ_z(O_I)	½+Δ_x(O_I)					
O_{III}	Δ_z(O_I)	½+Δ_x(O_I)	½+Δ_x(O_I)					

*) $i \neq j$.

Table 1A-2-004. $KNbO_3$. Lattice parameters and volume of unit cell [54Shi1]. a', b' : lattice parameters of pseudotetragonal cell.

T [°C]	$a' = c'$ [Å]	b' [Å]	b'/a'	β	V [Å^3]
25	4.0375	3.9711	1.0167	90°15'	64.73
125	4.0374	3.9797	1.0145	90°15'	64.87
185	4.0363	3.9830	1.0134	90°13'	64.89
205	4.0369	3.9839	1.0133	90°14'	64.93
	$a = b$	c	c/a		
220	3.9972	4.0636	1.0166		64.92
230	3.9978	4.0640	1.0166		64.95
270	3.9992	1.0647	1.0164		65.01
320	4.0023	4.0639	1.0154		65.10
375	4.0048	4.0620	1.0143		65.15
410	4.0080	4.0567	1.0122		65.18
425	4.0214		.		65.03
450	4.0225				65.09
510	4.0252				65.22

Table 1A-2-005. $KNbO_3$. Electromechanical constants [74Wie]. Orthorhombic phase.

Temperature T		25 °C	215 °C	
Density	ρ	4.62	4.605	[$\cdot 10^3$ kg m^{-3}]
Dielectric constants	$\kappa_{11}^{\mathbf{S}}$	37(2)	72(5)	
	$\kappa_{22}^{\mathbf{S}}$	780(50)	610(40)	
	$\kappa_{33}^{\mathbf{S}}$	24(2)	–	
	$\kappa_{11}^{\mathbf{T}}$	160(10)	1000(80)	
	$\kappa_{22}^{\mathbf{T}}$	1000(80)	700(40)	
	$\kappa_{33}^{\mathbf{T}}$	55(5)	125(10)	
Stiffness constants	$c_{11}^{\boldsymbol{E}}$	2.26(2)	2.20(3)	[$\cdot 10^{11}$ N m^{-2}]
	$c_{22}^{\boldsymbol{E}}$	2.70(2)	2.48(3)	
	$c_{33}^{\boldsymbol{D}}$	2.80(4)	2.60(4)	
	$c_{44}^{\boldsymbol{E}}$	0.743(5)	0.805(5)	
	$c_{44}^{\boldsymbol{D}}$	0.940(5)	0.925(10)	
	$c_{55}^{\boldsymbol{E}}$	0.250(2)	0.069(1)	
	$c_{55}^{\boldsymbol{D}}$	1.135(10)	0.955(10)	
-	$c_{66}^{\boldsymbol{E}} = c_{66}^{\boldsymbol{D}}$	0.955(10)	–	
	$c_{12}^{\boldsymbol{E}}$	0.96(3)		–
Piezoelectric constants	e_{15}	5.30(15)	7.5(4)	[C m^{-2}]
	d_{15}	21.5(5)	110(5)	[$\cdot 10^{-11}$ C N^{-1}]
	e_{24}	11.7(4)	8.0(5)	[C m^{-2}]
	d_{24}	15.9(5)	10.0(5)	[$\cdot 10^{-11}$ C N^{-1}]
Coupling constants	k_{15}	0.882(4)	0.965(4)	
	k_{24}	0.46(1)	0.360(15)	

Table 1A-2-006. $KNbO_3$. Dielectric constant $\kappa^{\mathbf{S}}_{ij}$, stiffness constant $c^{\boldsymbol{E}}_{\lambda\mu}$ and piezoelectric constant $e_{i\lambda}$ [93Zgo]. T = 22 °C.

$\kappa^{\mathbf{S}}_{11}$	34(2)		$c^{\boldsymbol{E}}_{44}$	0.743(8)	$[\cdot 10^{11}\ \mathrm{N\,m^{-2}}]$
$\kappa^{\mathbf{S}}_{22}$	780(22)		$c^{\boldsymbol{E}}_{55}$	0.25	$[\cdot 10^{11}\ \mathrm{N\,m^{-2}}]$
$\kappa^{\mathbf{S}}_{33}$	24(2)		$c^{\boldsymbol{E}}_{66}$	0.955(10)	$[\cdot 10^{11}\ \mathrm{N\,m^{-2}}]$
$c^{\boldsymbol{E}}_{11}$	2.26(3)	$[\cdot 10^{11}\ \mathrm{N\,m^{-2}}]$	e_{31}	2.46(20)	$[\mathrm{C\,m^{-2}}]$
$c^{\boldsymbol{E}}_{12}$	0.96(5)	$[\cdot 10^{11}\ \mathrm{N\,m^{-2}}]$	e_{32}	–1.1(7)	$[\mathrm{C\,m^{-2}}]$
$c^{\boldsymbol{E}}_{13}$	0.68(7)	$[\cdot 10^{11}\ \mathrm{N\,m^{-2}}]$	e_{33}	4.4(3)	$[\mathrm{C\,m^{-2}}]$
$c^{\boldsymbol{E}}_{22}$	2.70(3)	$[\cdot 10^{11}\ \mathrm{N\,m^{-2}}]$	e_{15}	5.16(12)	$[\mathrm{C\,m^{-2}}]$
$c^{\boldsymbol{E}}_{23}$	1.01(3)	$[\cdot 10^{11}\ \mathrm{N\,m^{-2}}]$	e_{25}	11.7(44)	$[\mathrm{C\,m^{-2}}]$
$c^{\boldsymbol{E}}_{33}$	1.86(5)	$[\cdot 10^{11}\ \mathrm{N\,m^{-2}}]$			

Table 1A-2-007. $KNbO_3$. Transition heats and transition entropies [54Shi2].

Transition	ΔQ_m [J mol^{-1}]	ΔS_m [J K^{-1} mol^{-1}]
IV $\rightarrow$ III	134	0.50
III $\rightarrow$ II	355	0.71
II $\rightarrow$ I	794	1.17

Table 1A-2-008. $KNbO_3$. Elastic stiffness constant at RT measured by Brillouin scattering [81Cam].

c_{11}	c_{22}	c_{12}	c_{66}	Ref.
[$\cdot 10^{11}$ N m^{-2}]				
2.26	2.70	0.96	0.95	74Wie
1.43	4.02	0.85	0.94	81Cam

Table 1A-2-009. $KNbO_3$. n vs. λ at RT [74Uem].

λ [nm]	n_a	n_b	n_c
488.0	2.3526	2.4190	2.2275
514.5	2.3329	2.3941	2.2116
532.1	2.3224	2.3807	2.2029
632.8	2.2799	2.3291	2.1685
1064.2	2.2200	2.2574	2.1196

Table 1A-2-010. $KNbO_3$. V_π, $r_{i\lambda}$, $\rho_{i\lambda}$ [74Gun]. λ = 633 nm. Additional data sources: $r_{42}^{T} < 0$ is from [89Ing] and values of r_{33}^{S}, r_{13}^{S}, r_{23}^{S} and r_{51}^{S} are from [76Gun].

iλ	V_π^T [kV]	V_π^S [kV]	$r_{i\lambda}^T$ [$\cdot 10^{-12}$ m V^{-1}]	$r_{i\lambda}^S$ [$\cdot 10^{-12}$ m V^{-1}]	$\rho_{i\lambda}^T$ [m^2 C^{-1}]	$\rho_{i\lambda}^S$ [m^2 C^{-1}]
33	–	–	+64(5)	25(8)	+13(2)	–
13	–	–	+28(2)	10(2)	+5.8(90)	–
23	–	–	≈ +1.3(5)	2(1)	+0.3(2)	–
42	0.15(2)	0.21(3)	–380(50)	270(40)	4.3(8)	4.0(8)
51	0.55(7)	–	105(13)	23(3)	7.4(15)	–
a = 33–$(n_2/n_3)^3$ 23	0.93(5)	2.1(3)	+65(4)	30(4)	13(2)	15(3)
b = 33–$(n_1/n_3)^3$ 13	2.1(1)	4.2(5)	+30(2)	15(2)	6.2(1)	7.3(15)
c = 13–$(n_2/n_1)^3$ 23	2.1(1)	4.3(7)	+26(2)	12(2)	5.6(9)	5.9(14)

$(n_1/n_3)^3 = 1.163$, $(n_2/n_3)^3 = 1.239$, $(n_2/n_1)^3 = 1.066$.

Table 1A-2-011. $KNbO_3$. Elastooptic constant $p_{\lambda\mu}^{\boldsymbol{E}}$ and electrooptic constant $r_{i\lambda}^{\boldsymbol{S}}$ [93Zgo]. T = 22 °C. λ = 633 nm.

$p_{11}^{\boldsymbol{E}}$	–0.20(4)	$p_{33}^{\boldsymbol{E}}$	0.82(4)	
$p_{12}^{\boldsymbol{E}}$	0.11(3)	$p_{44}^{\boldsymbol{E}}$	0.57(15)	
$p_{13}^{\boldsymbol{E}}$	0.55(5)	$p_{55}^{\boldsymbol{E}}$	0.45(10)	
$p_{21}^{\boldsymbol{E}}$	–0.13(3)	$r_{13}^{\boldsymbol{S}}$	21(2)	$[\cdot 10^{-12}\ \mathrm{m\,V^{-1}}]$
$p_{22}^{\boldsymbol{E}}$	0.23(3)	$r_{23}^{\boldsymbol{S}}$	7.1(7)	$[\cdot 10^{-12}\ \mathrm{m\,V^{-1}}]$
$p_{23}^{\boldsymbol{E}}$	0.16(2)	$r_{33}^{\boldsymbol{S}}$	35(2)	$[\cdot 10^{-12}\ \mathrm{m\,V^{-1}}]$
$p_{31}^{\boldsymbol{E}}$	0.64(11)	$r_{42}^{\boldsymbol{S}}$	360(30)	$[\cdot 10^{-12}\ \mathrm{m\,V^{-1}}]$
$p_{32}^{\boldsymbol{E}}$	0.15(3)	$r_{51}^{\boldsymbol{S}}$	27.8(30)	$[\cdot 10^{-12}\ \mathrm{m\,V^{-1}}]$

Table 1A-2-012. $KNbO_3$. X-ray photoelectron spectroscopic determination of core level binding energies relative to the O 1s level taken at 531.0 eV [78Per].

Level	Binding energy [eV]	Level	Binding energy [eV]
O 1s	531.00	Nb $4p_{1/2}$	38.0(1)
Nb $3d_{3/2}$	210.9(1)	Nb $4p_{3/2}$	36.3(1)
Nb $3d_{5/2}$	208.1(1)	K 3s	33.4(1)
K $2p_{1/2}$	295.6(1)	O 2s	22.8(1)
K $2p_{3/2}$	297.8(1)	K $3p_{1/2}$, K $3p_{3/2}$	17.3(1)

Table 1A-2-013. $KNbO_3$. NQR spectrum [54Cot]. The measured frequency ratios intersect the calculated ratios in a straight line at constant $\eta = 0.806(2)$. η: asymmetry parameter.

Crystal structure	f [MHz]	Measured ratio	Calculated ratio	Identification	e^2qQ/h [MHz]
			$\eta = 0.806$		
Orthorhombic	3.648			(9/2, 7/2)	23.12(5)
(20°C)		1.204	1.204		
	3.030			(3/2, 1/2)	
		1.196	1.196		
	2.527			(7/2, 5/2)	
		1.214	1.213		
	2.085			(5/2, 3/2)	
			$\eta = 0.0$		
Rhombohedral	2.674			(9/2, 7/2)	16.0(1)
(−196°C)		1.335	1.333		
	2.004			(7/2, 5/2)	
		1.503	1.500		
	1.335			(5/2, 3/2)	

Table 1A-2-014. $KNbO_3$:Fe^{3+}. Spin Hamiltonian parameters. A: Fe^{3+} ion at a Nb^{5+} site surrounded by 6 oxygens at T = 300 K; B: charge compensated center at T = 300 K [76Sie, 75Sie].

	A	*B*
b_{20}	± 5338(2) MHz	± 22(2)GHz
b_{40}	± 170(2) MHz	± 4(1) GHz
b_{22}	± 879(8) MHz	± 4.0(1) GHz
b_{42}	± 69(27) MHz	
b_{44}	± 730(28) MHz	
g	2.0053	
D	± 5338(2) MHz	
E	± 293(3) MHz	
$a = 2/5\ b_{44}$	± 292(12) MHz	

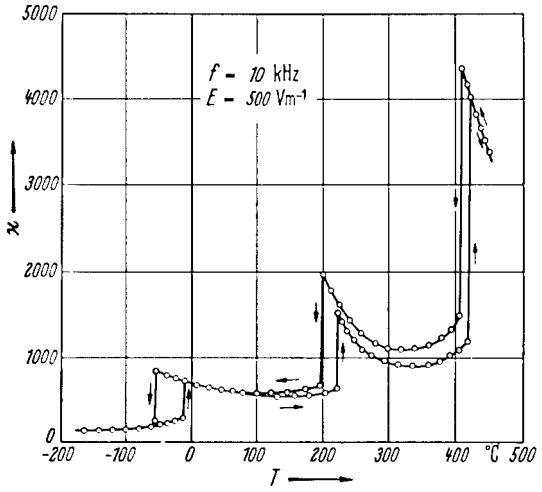

Fig. 1A-2-001. $KNbO_3$. κ vs. T [54Shi2].

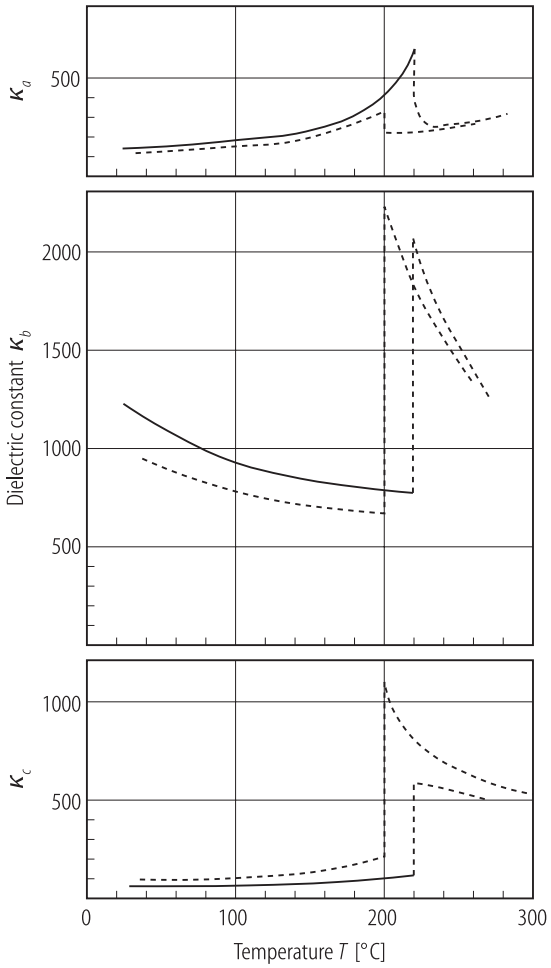

Fig. 1A-2-002. $KNbO_3$. κ_a, κ_b, κ_c vs. T [74Fuk2]. f = 1 kHz.

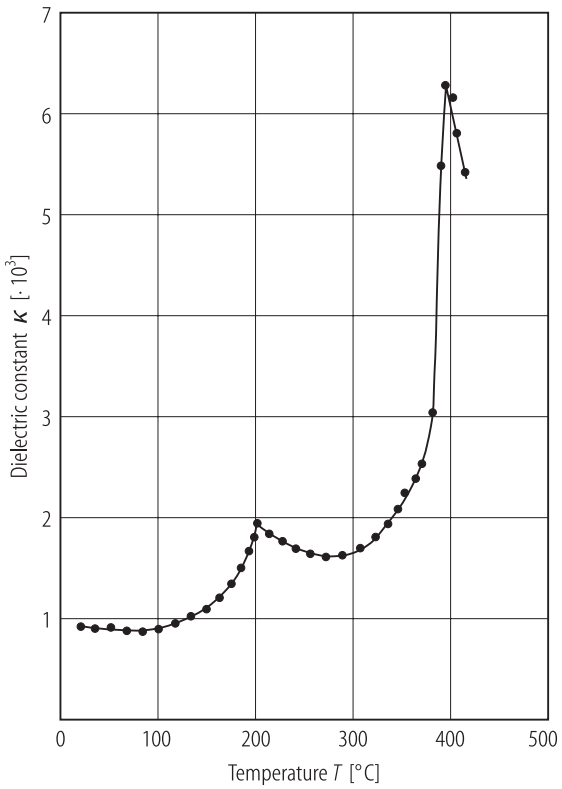

Fig. 1A-2-003. $KNbO_3$ (ceramics). κ vs. T [90Naz]. f = 1 kHz. The sample was prepared with sol-gel method.

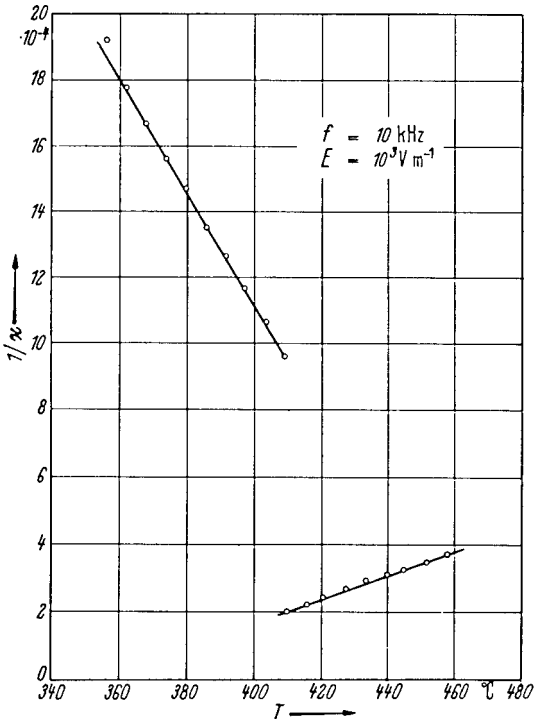

Fig. 1A-2-004. $KNbO_3$. κ^{-1} vs. T [56Tri].

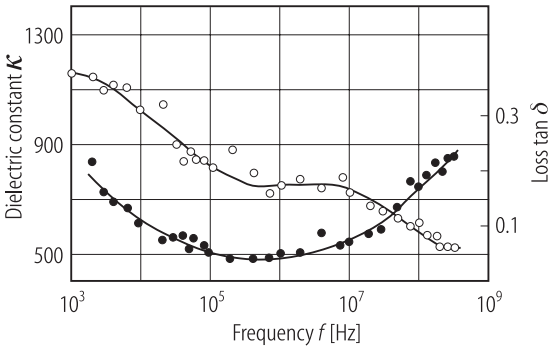

Fig. 1A-2-005. $KNbO_3$ (ceramics). κ, $\tan\delta$ vs. f [78Tur].
T = 25 °C.

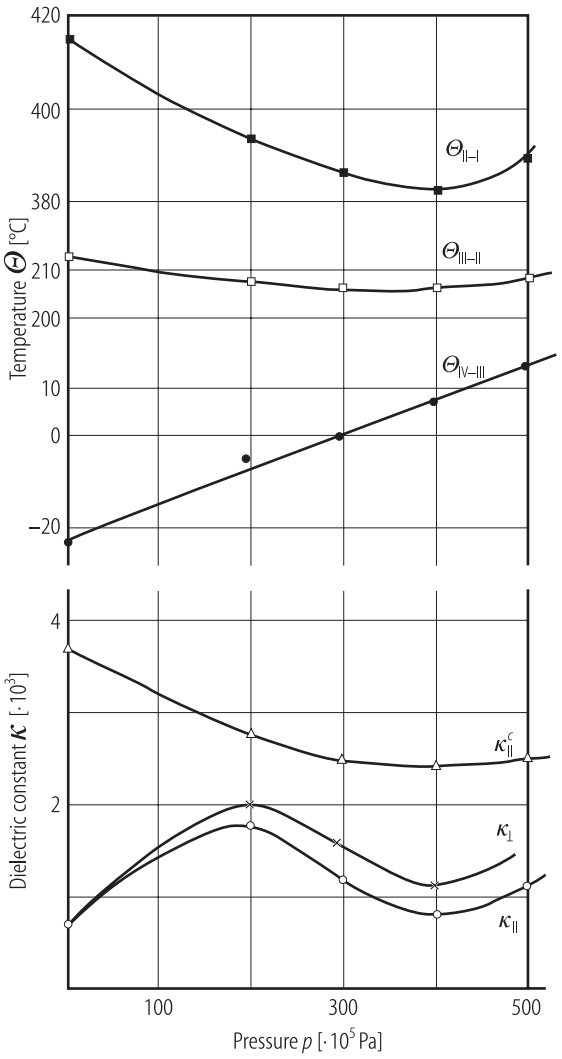

Fig. 1A-2-006. $KNbO_3$ (ceramics). $\Theta_{II–I}$, $\Theta_{III–II}$, $\Theta_{IV–III}$, $\kappa_{\parallel}^{c}$, $\kappa_{\parallel}$, $\kappa_{\perp}$ vs. p [78Tur]. $\kappa_{\parallel}^{c}$: κ at $\Theta_{II–I}$ at 16 kHz. $\kappa_{\parallel}$, $\kappa_{\perp}$: κ at RT at 1 kHz measured parallel and perpendicular to direction of hot-pressing. p: hot-pressing pressure.

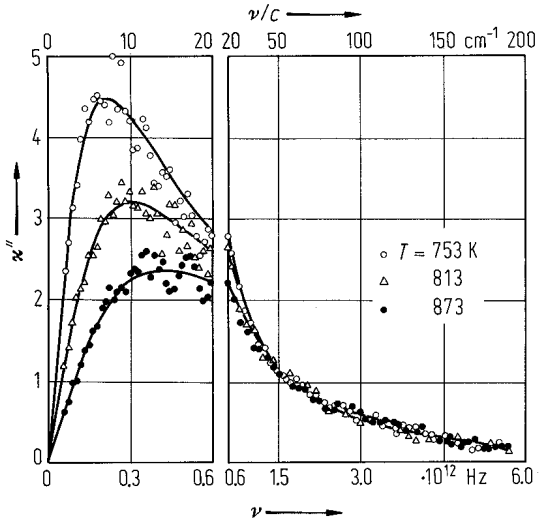

Fig. 1A-2-007. $KNbO_3$. κ'' vs. ν [86Vog]. Parameter: *T*. Obtained from the hyper-Raman spectra. Solid lines are the single-oscillator fits.

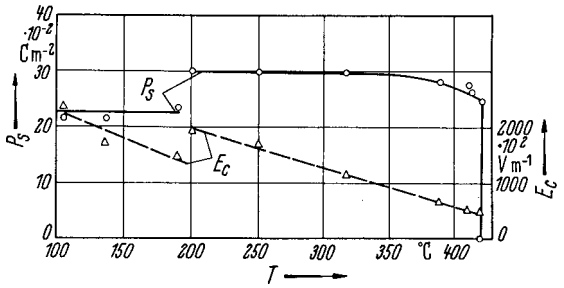

Fig. 1A-2-008. $KNbO_3$. P_s, E_c vs. T [56Tri]. Measurements were made by applying an electric field parallel to the pseudocubic [100] direction.

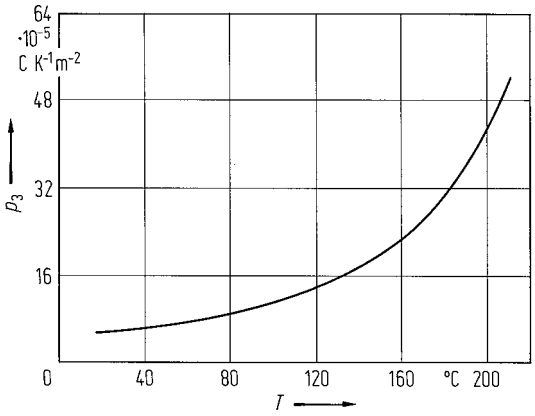

Fig. 1A-2-009. $KNbO_3$. p_3 vs. T [77Gun]. p_3: pyroelectric coefficient along [001] axis (the pseudocubic <110> direction). Relative errors were 20%. Single domain crystals were used.

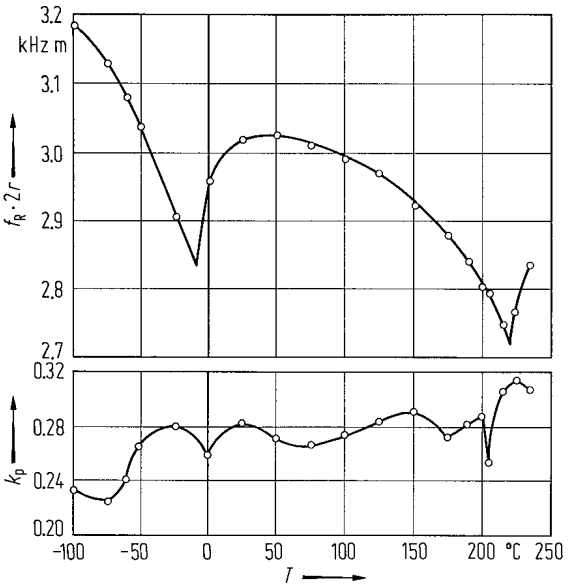

Fig. 1A-2-010. $KNbO_3$ (ceramics). k_p, $f_R \cdot 2r$ vs. T [59Ege]. k_p: planar electromechanical coupling factor. $f_R \cdot 2r$: radial frequency constant.

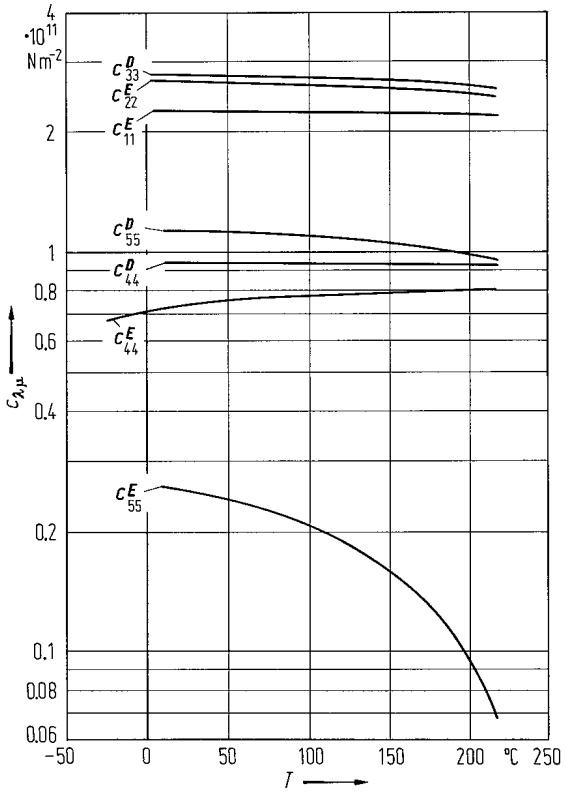

Fig. 1A-2-011. $KNbO_3$. $c_{\lambda\mu}$ vs. T [74Wie].

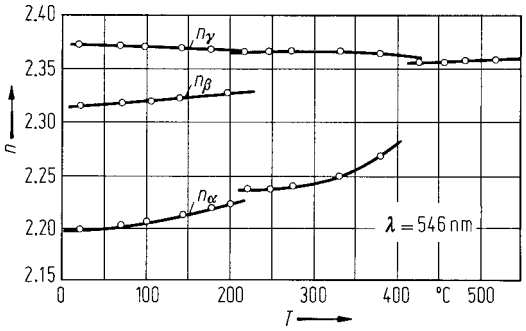

Fig. 1A-2-012. $KNbO_3$. n vs. T [70Wie]. n_α, n_β, n_γ : principal refractive indices.

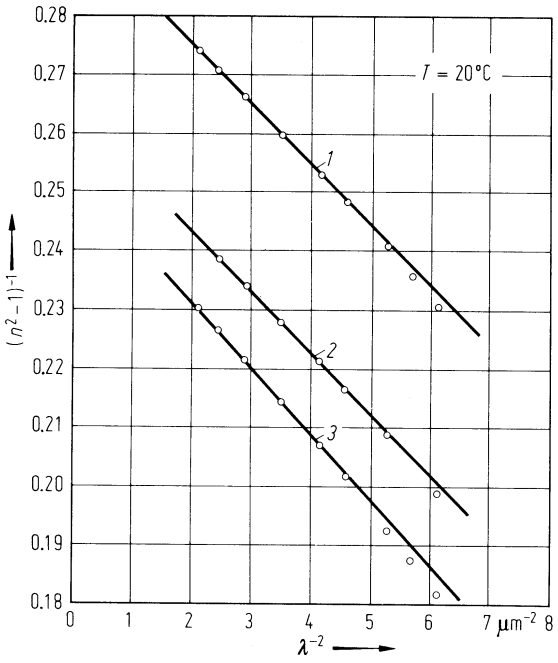

Fig. 1A-2-013. $KNbO_3$. $(n^2-1)^{-1}$ vs. λ^{-2} [70Wie]. Curve *1*: $(n_\alpha^2-1)^{-1}$, curve *2*: $(n_\beta^2-1)^{-1}$, curve *3*: $(n_\gamma^2-1)^{-1}$.

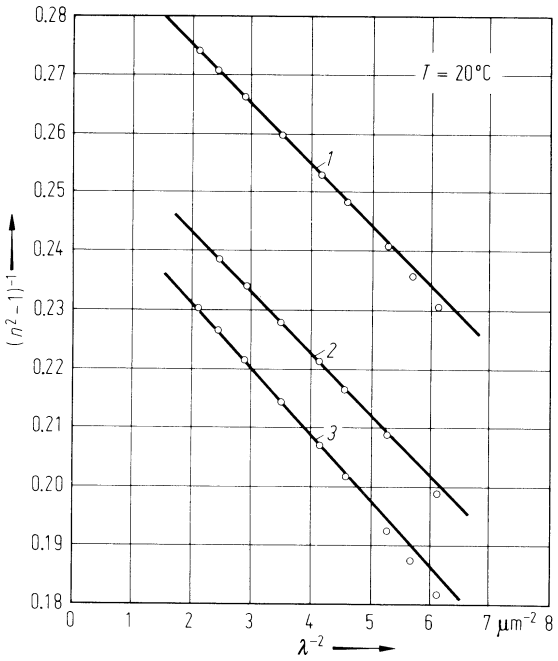

Fig. 1A-2-014. $KNbO_3$. Δn vs. T [70Wie]. $\Delta n_{\gamma\alpha} = n_\gamma - n_\alpha$, $\Delta n_{\beta\alpha} = n_\beta - n_\alpha$.

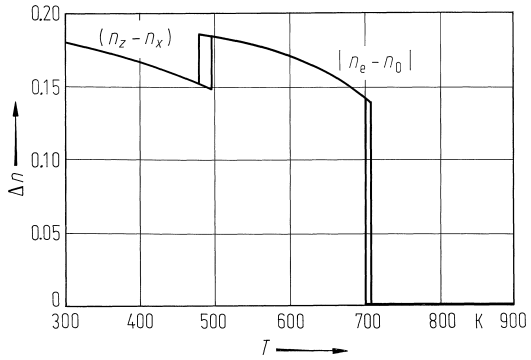

Fig. 1A-2-015. $KNbO_3$. Δn vs. T [84Kle]. λ = 589.3 nm.

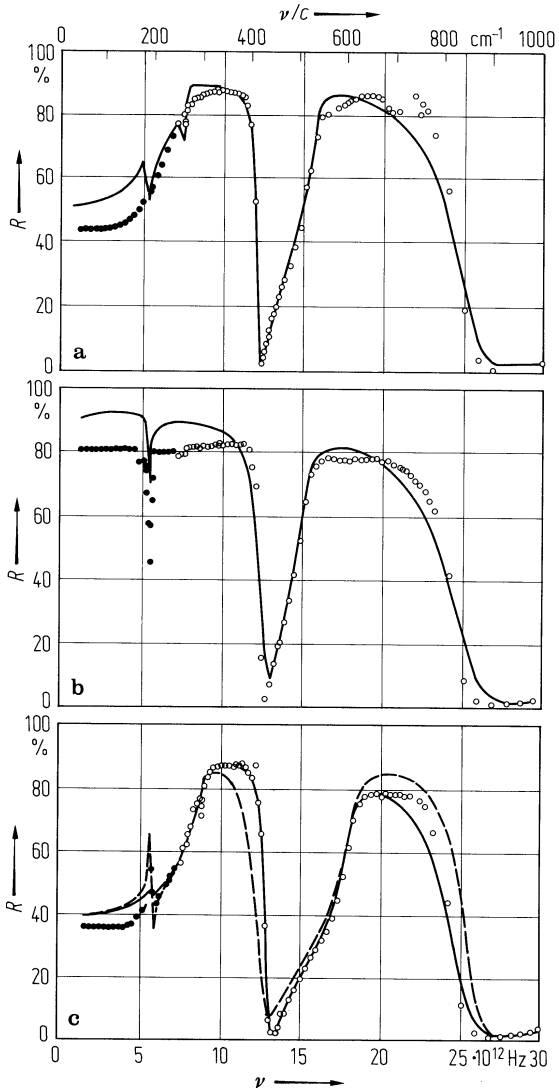

Fig. 1A-2-016. $KNbO_3$. R vs. ν at RT [76Boz1]. R : reflectivity, ν: infrared radiation frequency. Polarization of the radiation is along x in **(a)**, y in **(b)** and z in **(c)**. Open circles represent accurate data points. Full circles represent data with uncertain normalization errors. Continuous curve is derived from reflectivity analysis. Broken curve is derived from Raman data.

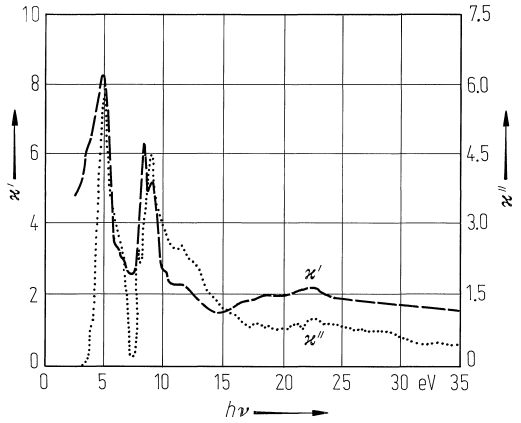

Fig. 1A-2-017. $KNbO_3$. κ' , κ'' vs. $h\nu$ [84Mam]. T = 300 K. $h\nu$: photon energy. κ' and κ'' were estimated from the reflectivity data using Kramers-Kronig relation.

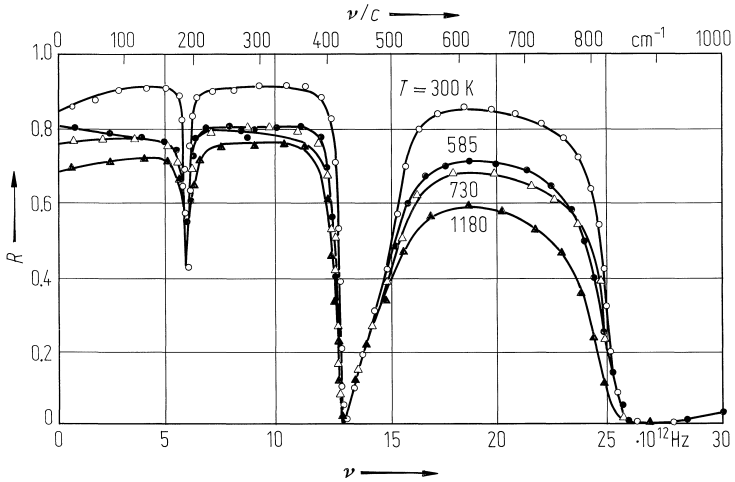

Fig. 1A-2-018. $KNbO_3$. R vs. ν [84Fon]. R: infrared reflectivity. Polarization of the radiation was chosen so that B_2 modes in phase III (orthorhombic phase, T = 300 K), E modes in phase II (tetragonal phase, T = 585 K) and F_{1u} modes in phase I (cubic phase, T = 730 and 1180 K) are observed, respectively.

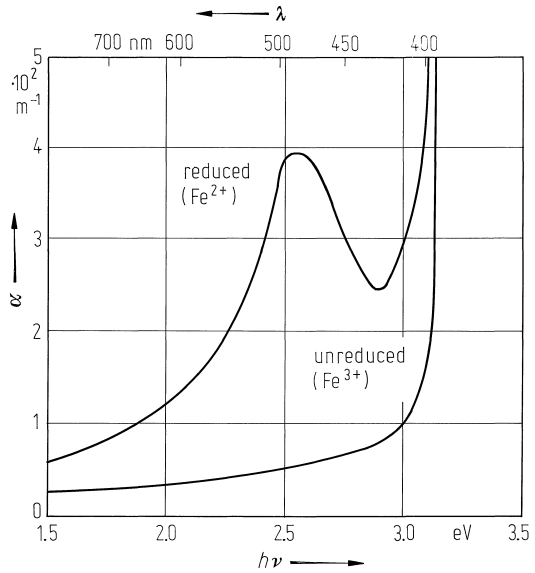

Fig. 1A-2-019. $KNbO_3$ (Fe doped). α vs. $h\nu$ [83Gun]. T = 300 K. α: optical absorption coefficient.

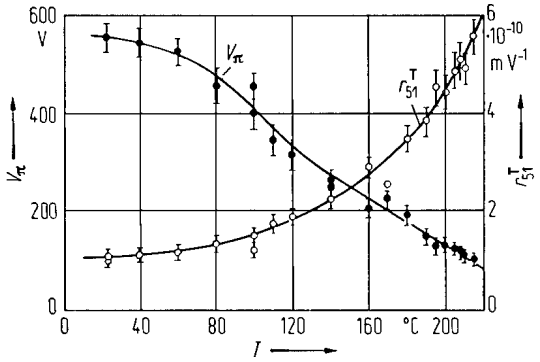

Fig. 1A-2-020. $KNbO_3$. V_π , r_{51}^T vs. T [74Gun]. V_π : half-wave voltage (λ = 633 nm).

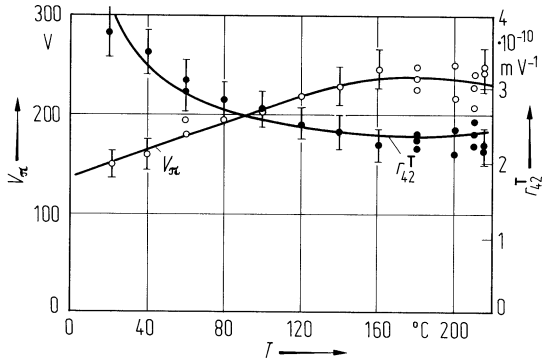

Fig. 1A-2-021. $KNbO_3$. V_π , r_a^T vs. T [74Gun]. V_π: half-wave voltage, $r_a^T = r_{33}^T - (n_2/n_3)^3 r_{23}^T$ (λ = 633 nm).

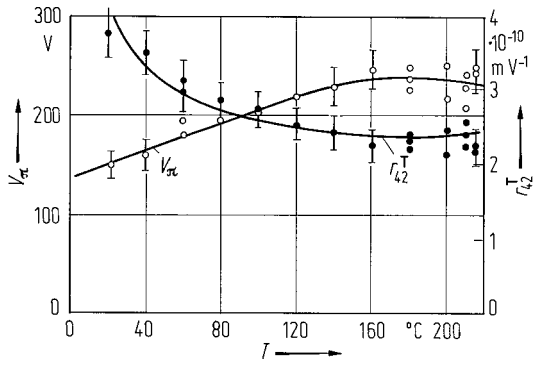

Fig. 1A-2-022. $KNbO_3$. V_π, r_{42}^T vs. T [74Gun]. V_π: half-wave voltage (λ = 633 nm).

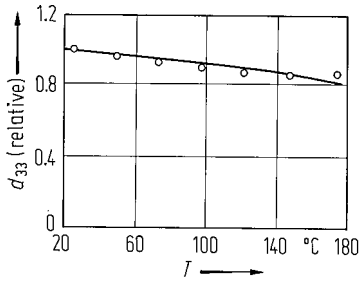

Fig. 1A-2-023. $KNbO_3$. d_{33} vs. T [74Uem]. d_{33}: relative nonlinear optical susceptibility.

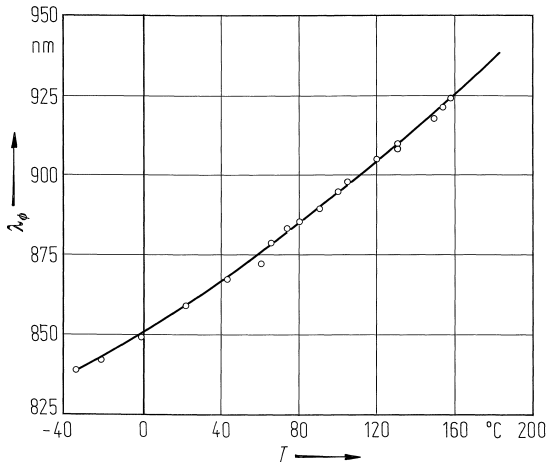

Fig. 1A-2-024. $KNbO_3$. λ_ϕ vs. T [83Bau]. λ_ϕ: SHG phase-matching wavelength for d_{32}.

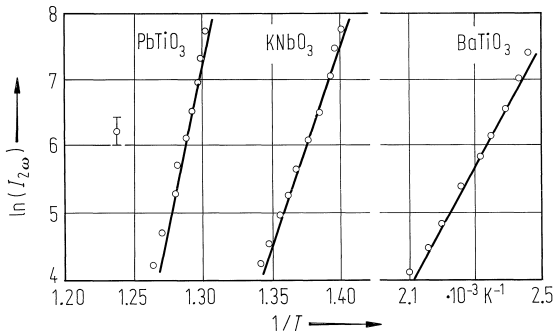

Fig. 1A-2-025. $KNbO_3$, $BaTiO_3$, $PbTiO_3$. ln($I_{2\omega}$ [arb. units]) vs. 1/T [81Lib]. $I_{2\omega}$: optical second harmonic intensity. λ = 1.064 μm.

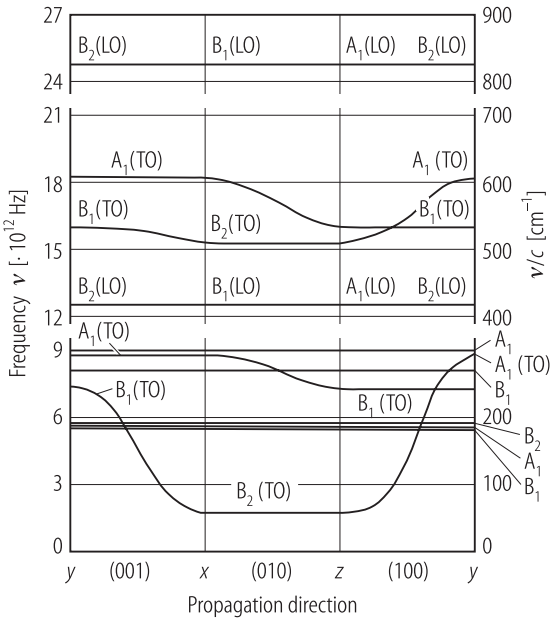

Fig. 1A-2-026. $KNbO_3$. ν vs. phonon propagation direction at RT [76Boz1]. ν: frequency of phonon modes obtained by Raman scattering. Curves are only schematic. Bold lines refer to the modes with strong infrared strength.

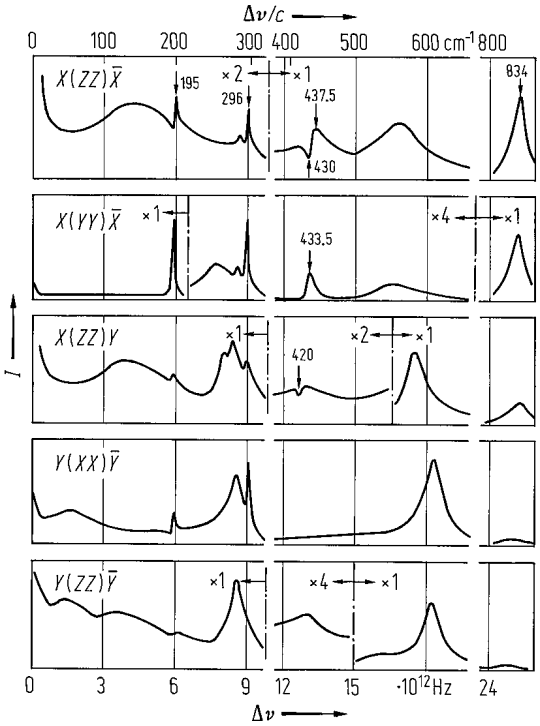

Fig. 1A-2-027. $KNbO_3$. Raman spectra for various scattering geometries at RT [76Qui]. Anomalous broad lines are seen in $X(ZZ)\overline{X}$ and *X(ZZ)Y*. Peak frequencies are indicated in the unit of cm^{-1}. See also [76Boz1].

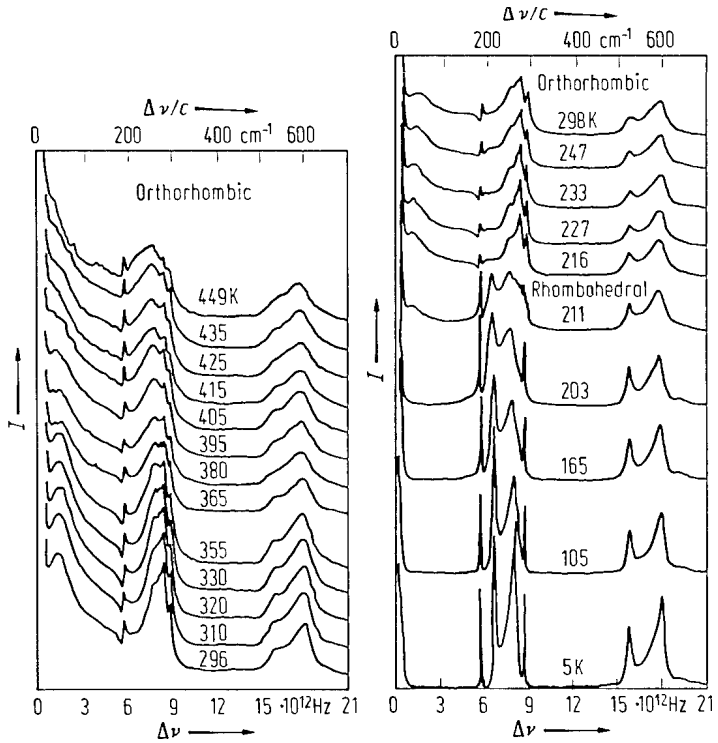

Fig. 1A-2-028. $KNbO_3$. I vs. $\Delta\nu$ [76Per]. I: Raman scattering intensity, $\Delta\nu$: Raman frequency shift. Parameter: T. The lowest $E(TO_1)$ branch is the temperature dependent ferroelectric mode while $E(TO_2)$, $E(TO_3)$ and $E(TO_4)$ are about 200, 280...290 and 530...550 cm^{-1}, respectively.

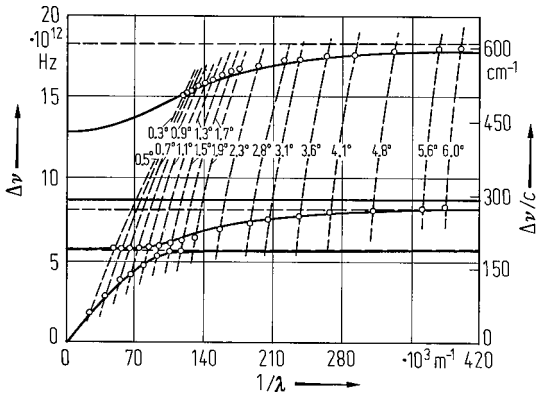

Fig. 1A-2-029. $KNbO_3$. Polariton dispersion curves at RT [75Fuk]. $\Delta\nu$: A_1 polariton frequency, $1/\lambda$: wave number of the polariton. Circles and solid curves are experimental and calculated curves, respectively. Horizontal broken lines indicate TO modes. Parameter: scattering angle. See also [76Cla].

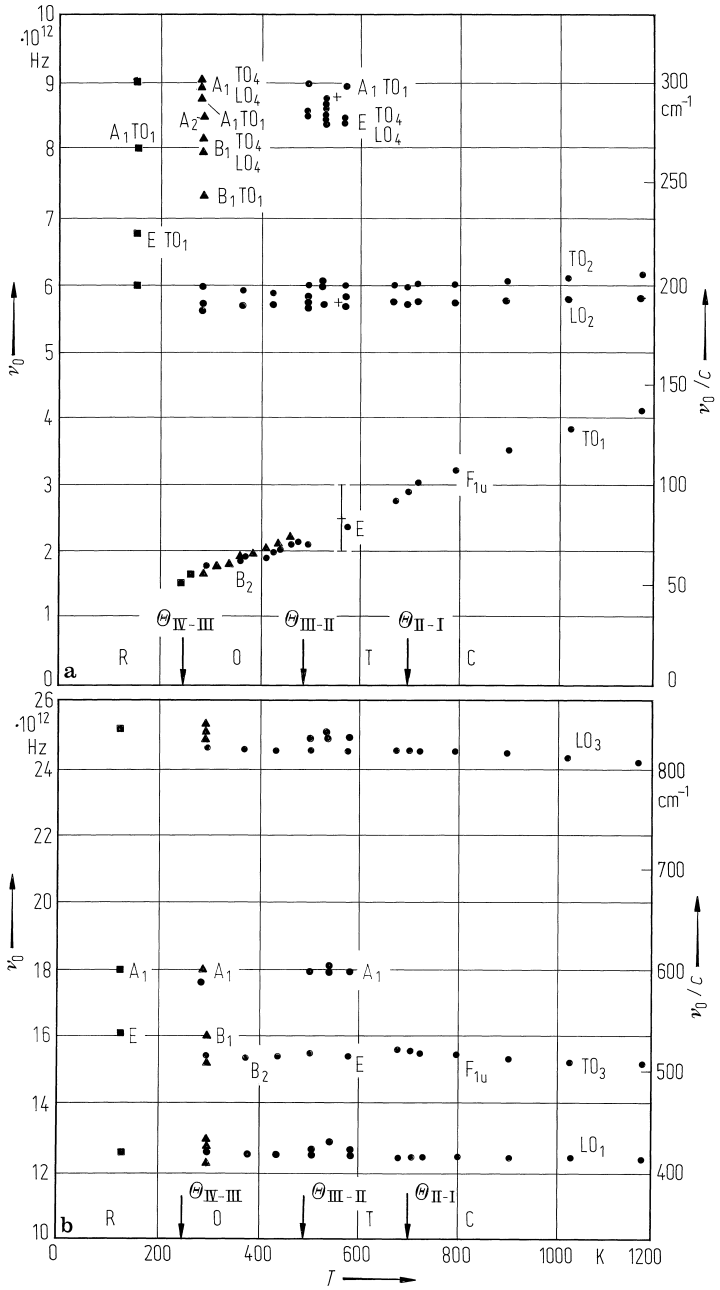

Fig. 1A-2-030. $KNbO_3$. ν_0 vs. T [84Fon]. ν_0: optical mode frequencies obtained from various experiments. **(a)** below 300 cm^{-1}. **(b)** above 300 cm^{-1}. Transverse (TO) and longitudinal (LO) modes and symmetries are indicated in the figure. Full circles: data from infrared spectroscopy [84Fon], full triangles: data from Raman and infrared spectroscopy [76Boz1, 76Boz2], full squares: data from Raman spectra [82Kug, 81Qui, 81Fon], plus signs: data from neutron scattering experiments [79Fon]. R, O, T and C mean rhombohedral, orthorhombic, tetragonal and cubic phase, respectively.

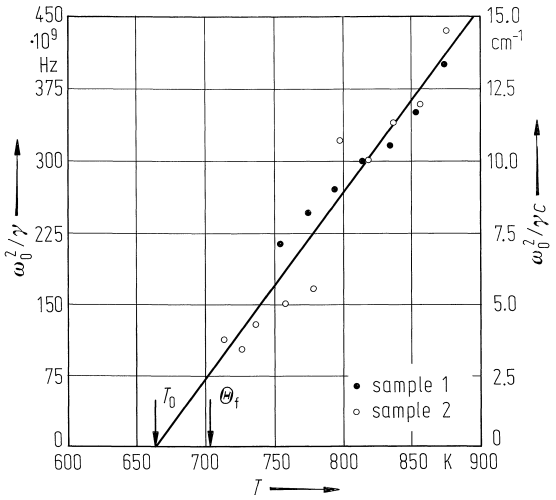

Fig. 1A-2-031. $KNbO_3$. ω_0^2/γ vs. T [86Vog]. ω_0: mode frequency. γ: damping constant. Obtained from the fitting of hyper-Raman spectrum to a damped harmonic oscillator formula.

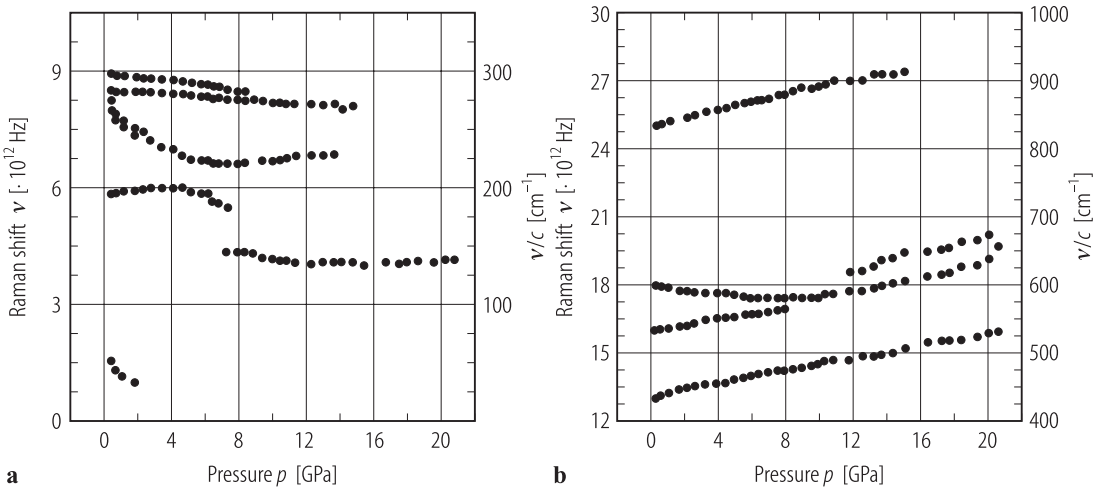

Fig. 1A-2-032. $KNbO_3$. ν vs. p [95She]. ν: Raman shift. T = RT. **(a)** $\nu < 9 \cdot 10^{12}$ Hz, **(b)** $\nu > 9 \cdot 10^{12}$ Hz.

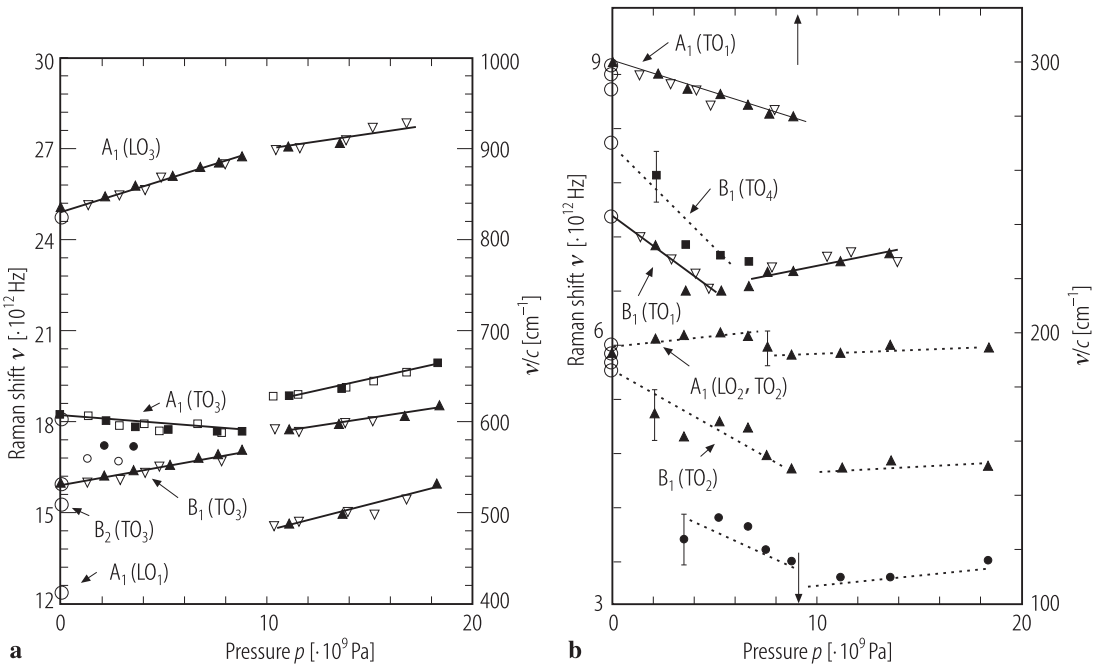

Fig. 1A-2-033. $KNbO_3$. ν vs. p [95Gou]. ν: Raman shift. T = RT. **(a)** $\nu < 3{\cdot}10^{13}$ Hz, **(b)** $\nu > 3{\cdot}10^{13}$ Hz. The vertical dashed lines indicate the proposed phase transition pressures. Large open circles at 0 GPa are data from [76Boz1]. Full symbols: increasing pressure runs, open symbols: decreasing pressure runs. Small closed circless in **(a):** not assigned. Small closed and open circles in **(b):** $B_2(LO_3)$. See [95Gou].

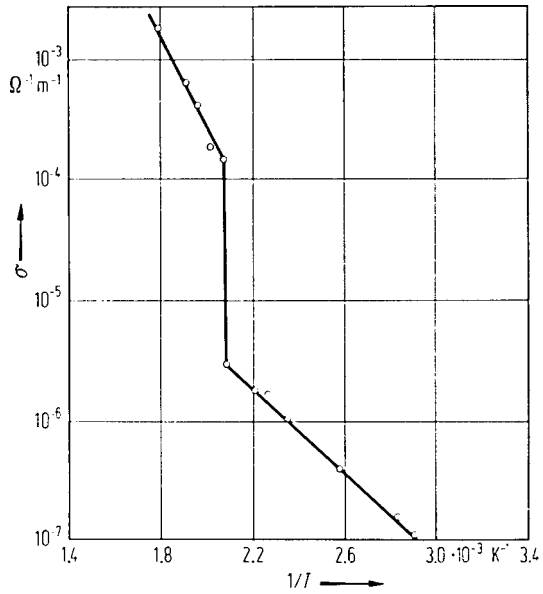

Fig. 1A-2-034. $KNbO_3$. σ vs. $1/T$ [62Gur]. σ : conductivity measured by two terminal methods with silver electrodes; applied field strength E = 1 MVm^{-1} for single crystal of 100 μm thickness.

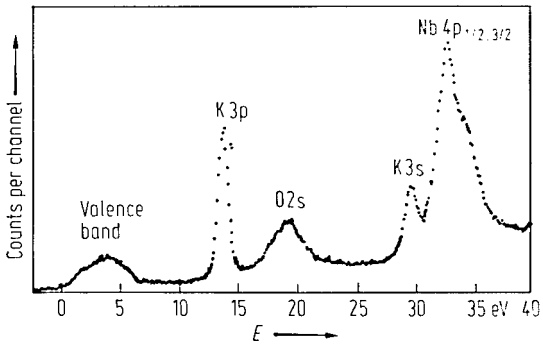

Fig. 1A-2-035. $KNbO_3$. X-ray photoelectron spectra for electron binding energies *E* below the valence band edge [78Per]. Incident X-ray: AlKα, resolution: 0.55 eV.

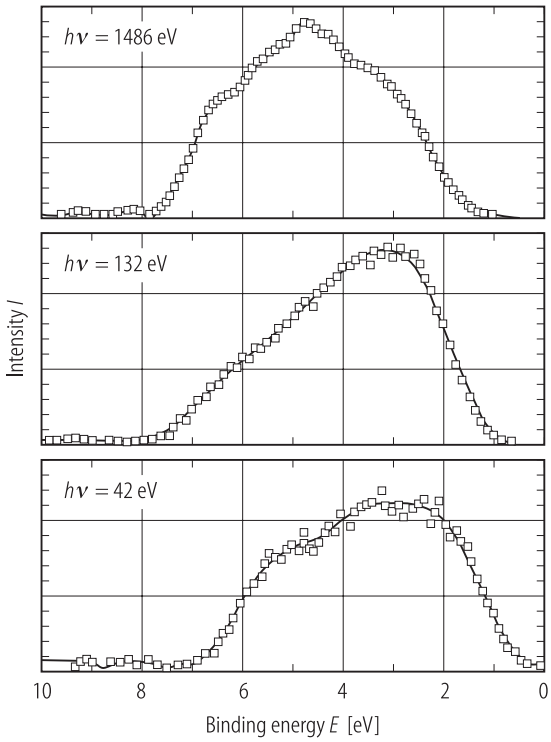

Fig. 1A-2-036. $KNbO_3$. X-ray photoelectron spectra for the valence band at RT [94Win]. Parameter: $h\nu$; photon energy of incident X-ray, monochromatized AlKα. *E*: binding energy below the valence band edge.

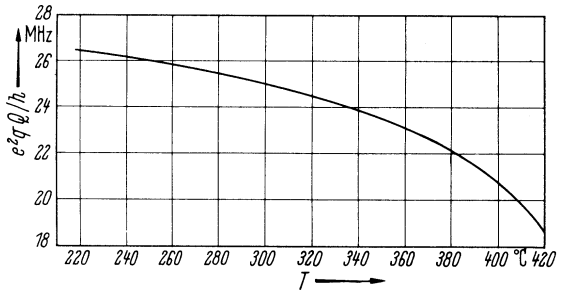

Fig. 1A-2-037. $KNbO_3$. e^2qQ/h of ^{93}Nb vs. T in phase II [61Hew].

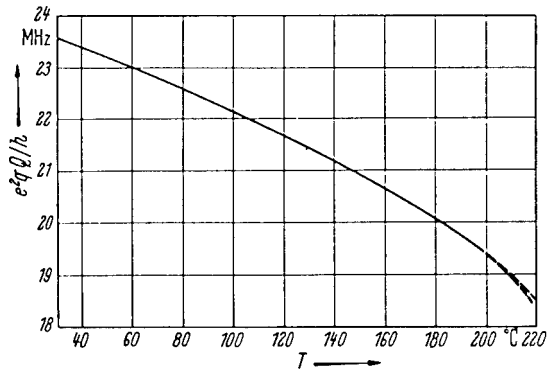

Fig. 1A-2-038. $KNbO_3$. e^2qQ/h of ^{93}Nb vs. T in phase III [61Hew].

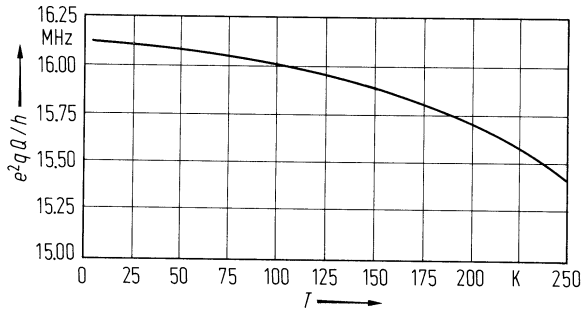

Fig. 1A-2-039. $KNbO_3$. e^2qQ/h of ^{93}Nb vs. T in phase IV [61Hew].

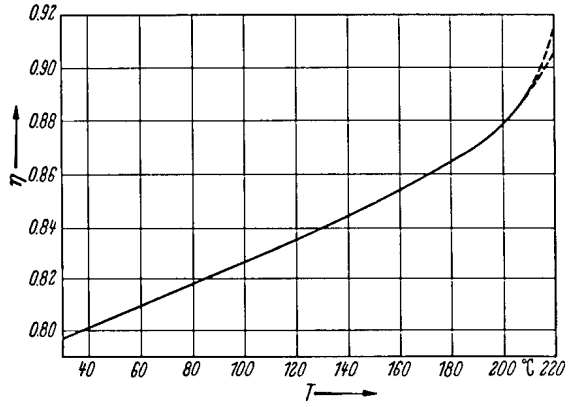

Fig. 1A-2-040. $KNbO_3$. η vs. T [61Hew]. η: asymmetry parameter.

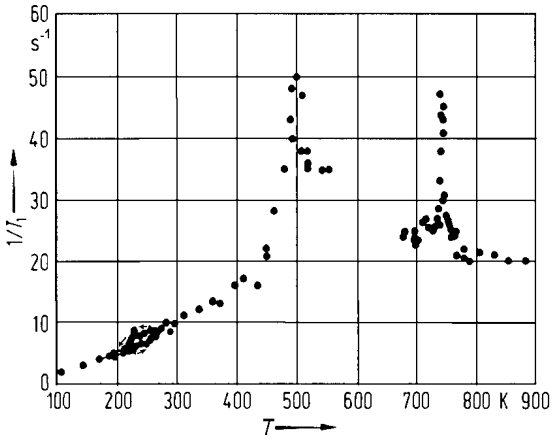

Fig. 1A-2-041. $KNbO_3$. $1/T_1$ vs. T [72Bon]. T_1: ^{93}Nb spin-lattice relaxation time. ν = 20 MHz. A temperature hysteresis was observed near Θ_{IV-III}.

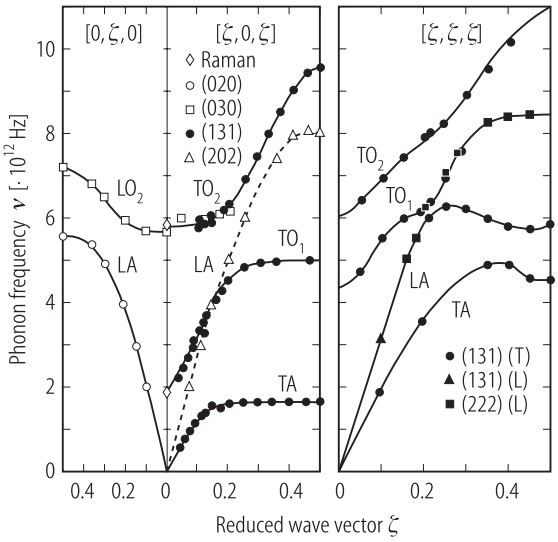

Fig. 1A-2-042. $KNbO_3$. ν vs. ζ [89Cur]. ν: phonon frequency, ζ: reduced wave vector coordinate. Diamonds: Raman scattering data. T = RT.

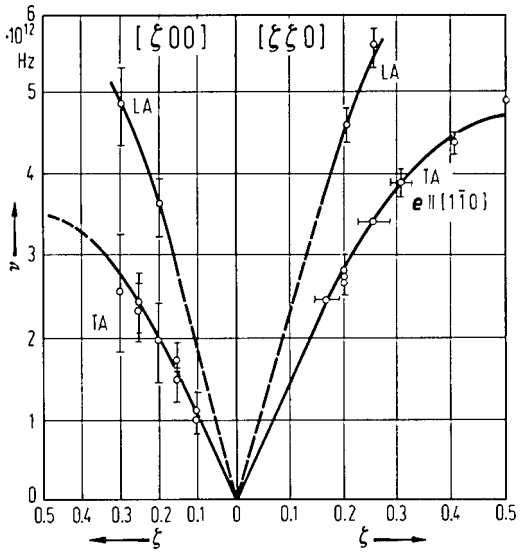

Fig. 1A-2-043. $KNbO_3$. ν vs. ζ [71Nun]. ν: phonon frequency, ζ: reduced wave vector coordinate. T = 460 °C.

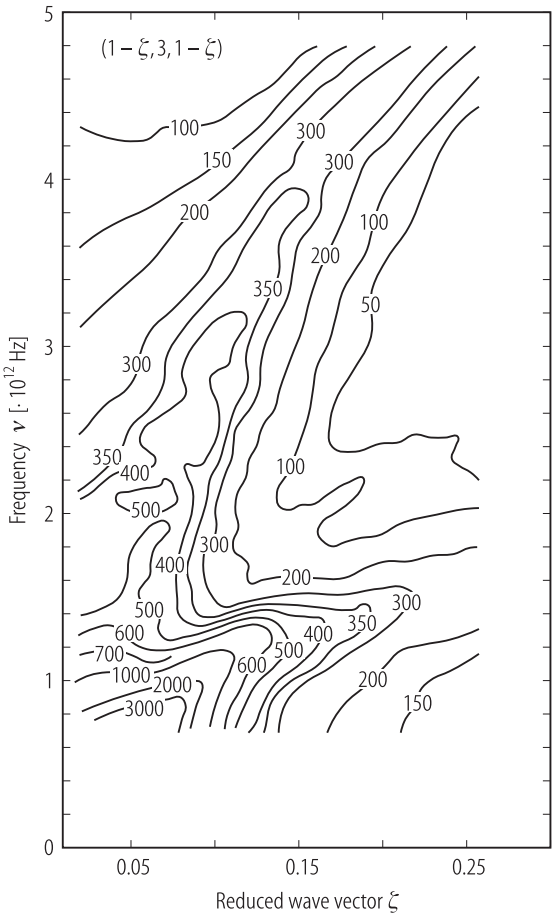

Fig. 1A-2-044. $KNbO_3$. Neutron intensity map [89Cur]. Constant-energy scans. ζ: reduced wave vector coordinate. T = RT.

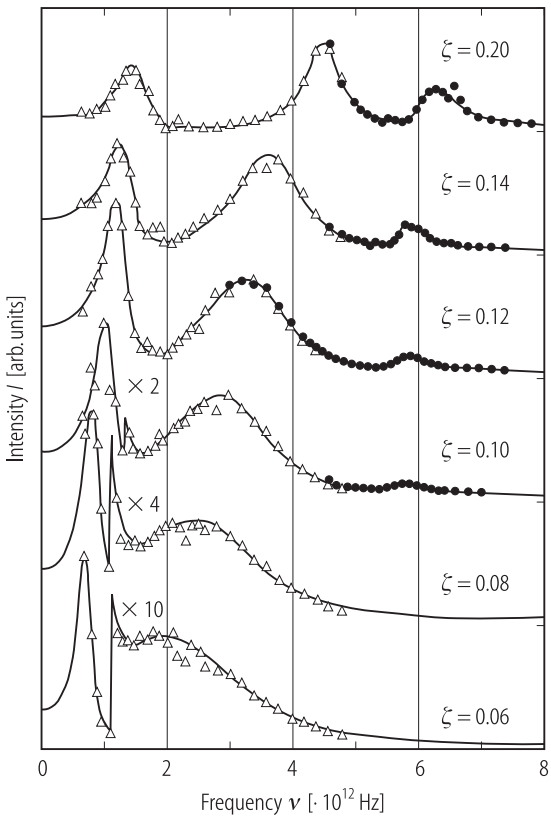

Fig. 1A-2-045. $KNbO_3$. I vs. ν [89Cur]. I: neutron scattering intensity at (1−ζ, 3, 1−ζ). Parameter: ζ. T = RT. Open triangles: data points replotted from Fig. 1A-2-044, full circles: data points derived from constant-Q measurements.

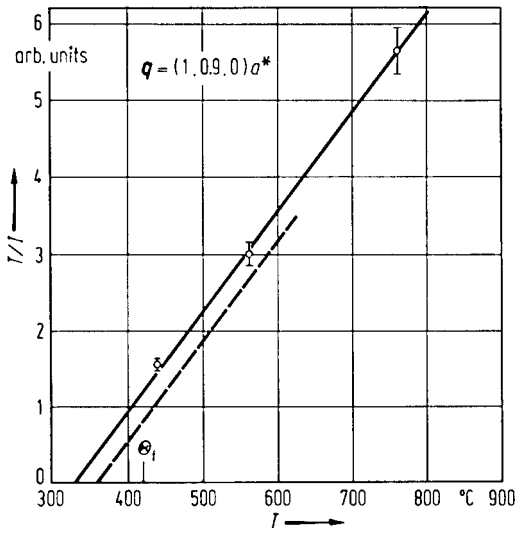

Fig. 1A-2-046. $KNbO_3$. *T/I* vs. *T* [71Num]. *I*: neutron scattering intensity of quasi-elastic peak integrated over ν at (1, 0.9, 0) in reciprocal lattice space. Broken line: temperature dependence extrapolated to $q = 0$.

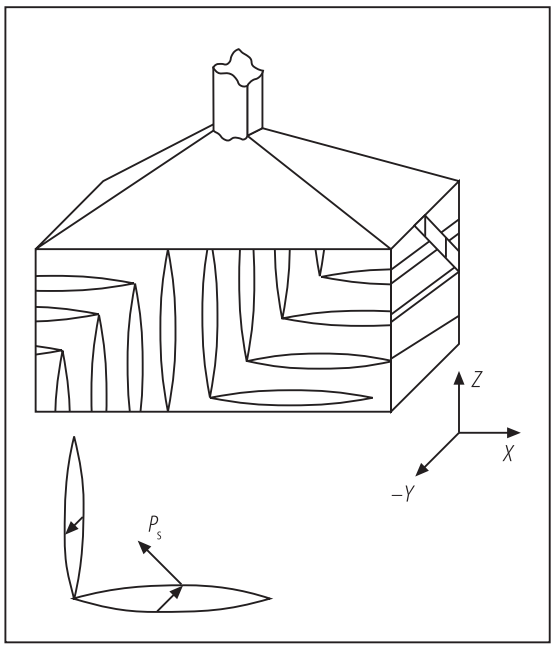

Fig. 1A-2-047. $KNbO_3$. Schematic diagram of the shape of as-grown crystal and domain structure [88Che].

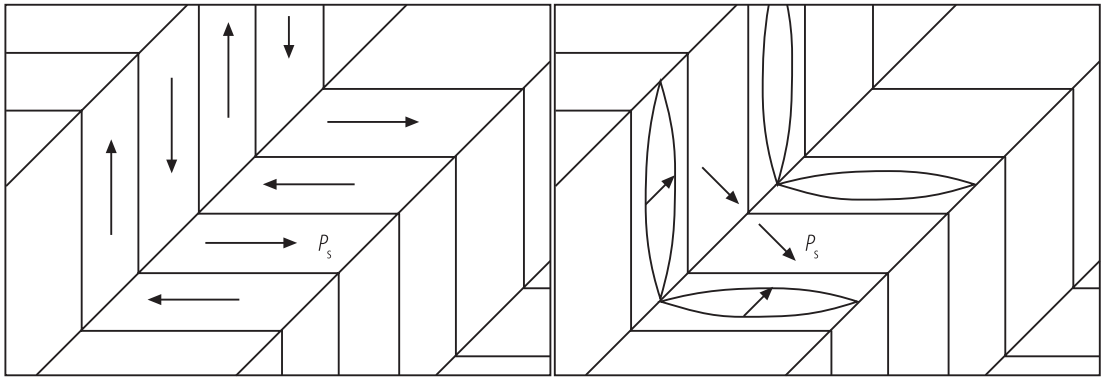

a **b**

Fig. 1A-2-048. $KNbO_3$. Schematic diagram of domain structure [88Che]. **(a)** teteragonal phase, **(b)** orthorhombic phase.

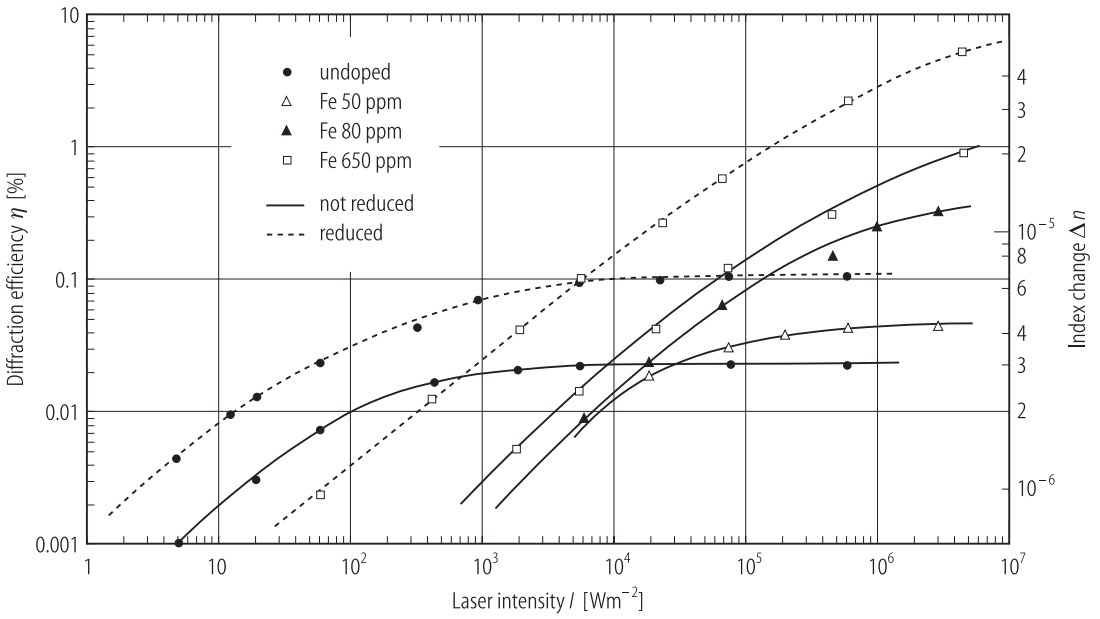

Fig. 1A-2-049. $KNbO_3$, $KNbO_3$:Fe (non reduced and reduced). η, Δn vs. I [78Gun]. η: saturation diffraction efficiency of the hologram for 1 mm thickness, Δn: refractive index change, I: Ar laser intensity for λ = 488 nm. Two beam mixing, beam angle 2θ = 13°. Diffraction efficiency was measured by a 1 mW He-Ne laser.

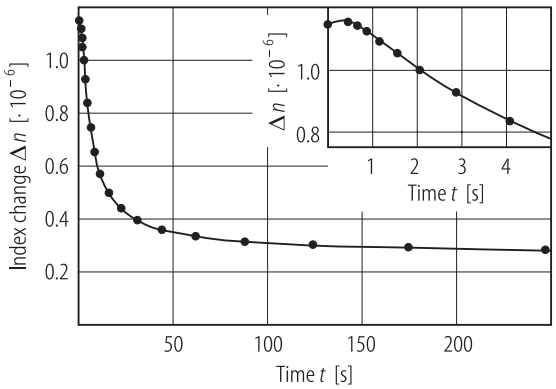

Fig. 1A-2-050. $KNbO_3$. Dark decay of the refractive index change Δn vs. t [90Mat]. Holographic grating was written with Ar-ion laser; λ = 514.5 nm, spacing of the interference fringes was 2.5 μm. After the light was switched off, the crystal was kept for a certain time interval t in absolute dark. Then the diffraction efficiency was measured with He-Ne laser, λ = 632.8 nm.

References

49Mat Matthias, B.T., Remeika, J.P.: Phys. Rev. **76** (1949) 1886.
51Woo Wood, E.A.: Acta Crystallogr. **4** (1951) 353.
54Cot Cotts, R.M., Knight, W.D.: Phys. Rev. **96** (1954) 1285.
54Shi1 Shirane, G., Newnham, R.E., Pepinsky, R.: Phys. Rev. **96** (1954) 581.
54Shi2 Shirane, G., Danner, H., Pavlovic, A., Pepinsky, R.: Phys. Rev. **93** (1954) 672.
55Rei Reisman, A., Holtzberg, F.: J. Am. Chem. Soc. **77** (1955) 2115.
56Tri Triebwasser, S.: Phys. Rev. **101** (1956) 993.
58Mil Miller, C.E.: J. Appl. Phys. **29** (1958) 233.
59Ege Egerton, L., Dillon, D.M.: J. Am. Ceram. Soc. **42** (1959) 438.
61Hew Hewitt, R.R.: Phys. Rev. **121** (1961) 45.
62Gur Gurevich, V.M.: Thesis of Candidate of Phys.-Math. Sciences, Moskva, 1962, cited in Gurevich, V.M.: Elektroprovodnost' Segnetoelektrikov, Moskva: Izdatel'stvo Komiteta Standartov, Mer i Izmeritel'nykh Priboroy pri Sovete Ministrov SSSR 1969; Electric Conductivity of Ferroelectrics, Jerusalem: Israel Program for Scientific Translations 1971.
63Kat Katz, L., Ueda, R., Megaw, H.D.: Acta Crystallogr. **16** (1963) Suppl. A189.
67Kat Katz, L., Megaw, H.D.: Acta Crystallogr. **22** (1967) 639.
68Com1 Comes, R., Lambert, M., Cuinier, A.: C. R. Acad. Sci. (Paris), Ser. B **266** (1968) 959.
68Com2 Comes, R., Lambert, M., Cuinier, A.: Solid State Commun. **6** (1968) 715.
70Com Comes, R., Lambert, M., Guinier, A.: Acta Crystallogr., Sect. A **26** (1970) 244.
70Wie Wiesendanger, F.: Ferroelectrics **1** (1970) 141.
71Com Comes, R., Denoyer, F., Lambert, M.: J. Phys. (Paris) **32**, Suppl. C-5a (1971) 195.
71Des Deshmukh, K.G., Ingle, S.G.: J . Phys. D **4** (1971) 124.
71Hur Hurst, J.J., Linz, A.: Mater. Res. Bull. **6** (1971) 163.
71Nun Nunes, A.C., Axe, J.D., Shirane, G.: Ferroelectrics **2** (1971) 291.
72Bon Bonera, G., Borsa, F., Rigamonti, A.: J. Phys. (Paris) **33**, Suppl. C-2 (1972) 195.
72Fuk Fukuda, T., Uematsu, Y.: Jpn. J. Appl. Phys. **11** (1972) 163.
72Kat Katpatal, A.G., Deshmukh, K.G.: J. Phys. D **5** (1972) 1937.
72Pha Phatak, S.D., Srivastava, R.C., Subbarao, E.C.: Acta Crystallogr., Sect. A **28** (1972) 227.
73Hew Hewat, A.W.: J. Phys. C **6** (1973) 2559.
74Fuk1 Fukuda, T., Uematsu, Y., Ito, T.: J. Cryst. Growth **24**/**25** (1974) 450.
74Fuk2 Fukuda, T., Hirano, H., Uematsu, Y., Ito, T.: Jpn. J. Appl. Phys. **13** (1974) 1021.
74Gun Günter, P.: Opt. Commun. **11** (1974) 285.
74Uem Uematsu, Y.: Jpn. J. Appl. Phys. **13** (1974) 1362.
74Wie Wiesendanger, E.: Ferroelectrics **6** (1974) 263.
75Fuk Fukumoto, T., Okamoto, A., Hattori, T., Mitsuishi, A.: Solid State Commun. **17** (1975) 427.
75Sie Siegel, E., Urban, W., Mueller, K.A., Wiesendanger, E.: Phys. Lett. A **53** (1975) 415.
76Boz1 Bozinis, D.G., Hurrell, J.P.: Phys. Rev. B **13** (1976) 3109.
76Boz2 Bozinis, D.G., Scalabrin, A.: Proceedings of the Third International Conference on Light Scattering in Solids, Balkanski, M., Leite, R.C.C., Porto, S.P.S. (eds.), held in Campinas (1975), Paris: Flammarion Sciences 1976, p. 856.
76Cla Claus, R., Winter, F.X.: Proceedings of the Third International Conference on Light Scattering in Solids, Balkanski, M., Leite, R.C.C., Porto, S.P.S. (eds.), held in Campinas (1975), Paris: Flammarion Sciences 1976, p. 485.
76Gun Günter, P.: Electro-optics/Laser 76 (Jerrard, H. ed.), IPS Science and Technology Press, England (1976) 121.
76Mic Michel-Calendini, F.M., Castet, L.: Ferroelectrics **13** (1976) 367.
76Per Perry, C.H., Hayes, R.R., Tornberg, N.E.: Proceedings of the Third International Conference on Light Scattering in Solids, Balkanski, M., Leite, R.C.C., Porto, S.P.S. (eds.), held in Campinas (1975), Paris: Flammarion Sciences 1976, p. 812.
76Qui Quittet, A.M., Bell, M.I., Krauzman, M., Raccab, P.M.: Phys. Rev. B **14** (1976) 5068.

76Sie Siegel, E.: Ferroelectrics **13** (1976) 385.
77Gun Günter, P.: J. Appl. Phys. **48** (1977) 3475.
77Rae Raevskii, I.P., Malitskaya, M.A., Vuitsik, K.A., Prokopalo, O.I., Smotrakov, V.G., Fesenko, E.G.: Fiz. Tverd. Tela **19** (1977) 3589; Sov. Phys. Solid State (English Transl.) **19** (1977) 2097.
78Gun Günter, P., Micheron, F.: Ferroelectrics **18** (1978) 27.
78Han Handerek, J., Wróbel, Z., Wójcik, K., Ujma, Z.: Ferroelectrics **18** (1978) 127.
78Per Pertosa, P., Michel-Calendini, F.M.: Phys. Rev. B **17** (1978) 2011.
78Tur Turik, A.V., Tais'eva, V.A., Raevskii, I.P., Reznichenko, L.A., Prokopalo, O.I.: Izv. Akad. Nauk SSSR, Neorg. Mater. **14** (1978) 912; Inorg. Mater. (English Transl.) **14** (1978) 715.
79Fon Fontana, M.D., Dolling, G., Kugel, G.E., Carabatos, C.: Phys. Rev. B **20** (1979) 3850.
81Cam Camagni, P., Manara, A., Morrone, L.: Recent Developments in Condensed Matter Physics, Vol. 4, Devreese, J.T., Lemmens, L.F., Van Doren, V.E., Van Royen, J. (eds.), Low-Dimensional Systems, Phase Changes, and Experimental Techniques: 1st General Conference of the Condensed Matter Division of the European Physical Society, Antwerpen: Plenum Press 1981, p. 175.
81Fon Fontana, M.D., Kugel, G.E., Métrat, G., Carabatos, C.: Phys. Status Solidi (b) **103** (1981) 211.
81Lib Liberts, G.V., Fritsberg, V.Ya.: Phys. Status Solidi (a) **67** (1981) K81.
81Pro Prokopalo, O.I., Raevskii, I.P., Malitskaya, M.A., Popov, Yu.M., Smotrakov, V.G., Fesenko, E.G.: Ferroelectrics **34** (1981) 57.
81Qui Quittet, A.M., Servoin, J.L., Gervais, F.: J. Phys. (Paris) **42** (1981) 493.
82Kug Kugel, G.E., Fontana, M.D., Vamvakas, J., Carabatos, C., Theophanous, N.: Raman Spectroscopy; Linear and Nonlinear, Proceedings of the 8th International Conference, Lascombe, J., Huong, P.V. (eds.), Bordeaux: Wiley Heyden Ltd. 1982, p. 457.
83Bau Baumert, J.-C., Günter, P., Melchior, H.: Opt. Commun. **48** (1983) 215.
83Bur Bursill, L.A., Lin, P.J., Duan, F.: Philos. Mag. A **48** (1983) 953.
83Gun Günter, P.: Ferroelectrics **49** (1983) 39.
84Fon Fontana, M.D., Métrat, G., Servoin, J.L., Gervais, F.: J. Phys. C **16** (1984) 483.
84Kle Kleemann, W., Schäfer, F.J., Fontana, M.D.: Phys. Rev. B **30** (1984) 1148.
84Mam Mamédov, A.M., Godzhieva, L.S.: Fiz. Tverd. Tela **26** (1984) 2862; Sov. Phys. Solid State (English Transl.) **26** (1984) 1732.
86Vog Vogt, H., Fontana, M.D., Kugel, G.E., Günter, P.: Phys. Rev. B **34** (1986) 410.
86WuE Wu, E.T., Ratto, J.J., Oliver, J.R., Neurgaonkar, R.R.: Proceedings of the Sixth IEEE International Symposium on Applications of Ferroelectrics, Bethlehem, PA, June 1986 (The Institute of Electrical and Electronics Engineers, Inc., New York, 1986), p. 478.
87Sam Samara, G.A.: Ferroelectrics **73** (1987) 145.
88Che Chen, J., Wang, W.S., Li, Q., Feng, D.: Cryst. Res. Technol. **23** (1988) 747.
89Cur Currat, R., Buhay, H., Perry, C.H., Quittet, A.M.: Phys. Rev. B **40** (1989) 10741.
89Ing Ingold, M., Günter, P.: Ferroelectrics **94** (1989) 117.
89Pos Possenriede, E., Schirmer, O.F., Donnerberg, H.J., Hellermann, B.: J. Phys. Condens. Matter **1** (1989) 7267.
90Mat Matull, R., Hesse, H., Holtmann, L., Rupp, R.A.: Ferroelectrics **107** (1990) 47.
90Naz Nazeri-Eshghi, A., Kuang, A.X., Mackenzie J.D.: J. Mater. Sci. **25** (1990) 3333.
90Tut Tuttle, B.A., Bunker, B.C., Lamppa, D.L., Tissot, R.G., Yio, J.L.: Ceramic Transactions Vol. 11. Ceramic Thin and Thick Films, Hiremath, B.V. (ed.), (1990) 329.
90XuY Xu, Y.-N., Ching, W.Y., French, R.H.: Ferroelectrics **111** (1990) 23.
90Zha Zhang, L., Chandler, P.J., Toensend, P.D.: Ferroelectrics Lett. **11** (1990) 89.
91Cro Cross, L.E., Rossetti Jr., G.A.: J. Appl. Phys. **69** (1991) 896.
91Law Lawler, W.B., Sherman, C.J., Moharam, M.G.: J. Opt. Soc. Am. B **8** (1991) 2190.
91Ree Reeves, R.J., Jani, M.G., Jassemnejad, B., Powell, R.C., Mizell, G.J., Fay, W.: Phys. Rev. B **43** (1991) 71.

92Neu Neumann, T., Borstel, G., Scharfschwerdt, C., Neumann, M.: Phys. Rev. B **46** (1992) 10623.
93Flu Fluck, D., Jundt, D.H., Günter, P.: J. Appl. Phys. **74** (1993) 6023.
93Res Resta, R., Posternak, M., Baldereschi, A.: Phys. Rev. Lett. **70** (1993) 1010.
93Zgo Zgonik, M., Schlesser, R., Biaggio, I., Voit, E., Tsvherry, J., Günter, P.: J. Appl. Phys. **74** (1993) 1287.
94Der Derderian, G.J., Barrie, J.D., Aitchison, K.A., Adams, P.M., Mecartney, M.L.: J. Am. Ceram. Soc. **77** (1994) 820.
94Dou Douillard, L., Jollet, F., Bellin, C., Gautier, M., Duraud, J.P.: J. Phys. Condens. Matter **6** (1994) 5039.
94Kin King-Smith, R.D., Vanderbit, D.: Phys. Rev. B **49** (1994) 5828.
94Win Winiarski, A., Neumann, T., Mayer, B., Borstel, G., Neumann, M.: Phys. Status Solidi (b) **183** (1994) 475.
95Gop Gopalan, V., Raj, R.: J. Am. Ceram. Soc. **78** (1995) 1825.
95Gou Gourdain, D., Moya, E., Chervin, J.C., Canny, B., Pruzan, Ph.: Phys. Rev. B **52** (1995) 3108.
95She Shen, Z.X., Hu, Z.P., Chong, T.C., Beh, C.Y., Tang, S.H., Kuok, M.H.: Phys. Rev. B **52** (1995) 3976.
96Sin Singh, D.J.: Phys. Rev. B **53** (1996) 176.